CHEMISTRY OF MATERIALS
Cite This: Chem. Mater. 2019, 31, 407−418
Article
pubs.acs.org/cm

In Situ Mechanochemical Modulation of Carbon Nanotube Forest Growth

Nicholas T. Dee,[†] Mostafa Bedewy,[†,‡] Abhinav Rao,[†] Justin Beroz,[†] Byeongdu Lee,[§] Eric R. Meshot,[∥] Cécile A. C. Chazot,[†,⊥] Piran R. Kidambi,[†] Hangbo Zhao,[†] Thomas Serbowicz,[#] Kendall Teichert,[#] Prashant K. Purohit,[¶] and A. John Hart*[,†]

[†]Department of Mechanical Engineering and [⊥]Department of Materials Science and Engineering, Massachusetts Institute of Technology, Cambridge, Massachusetts 02139, United States

[‡]Department of Industrial Engineering and Department of Chemical and Petroleum Engineering, University of Pittsburgh, Pittsburgh, Pennsylvania 15261, United States

[§]X-ray Science Division, Argonne National Laboratory, 9700 South Cass Avenue, Lemont, Illinois 60439, United States

[∥]Physical and Life Sciences Directorate, Lawrence Livermore National Laboratory, 7000 East Avenue, Livermore, California 94550, United States

[#]Department of Mechanical Engineering, University of Michigan, Ann Arbor, Michigan 48109, United States

[¶]Department of Mechanical Engineering and Applied Mechanics, University of Pennsylvania, Philadelphia, Pennsylvania 19104, United States

Supporting Information

Downloaded via NORTHWESTERN UNIV on September 2, 2019 at 03:40:41 (UTC).
See https://pubs.acs.org/sharingguidelines for options on how to legitimately share published articles.

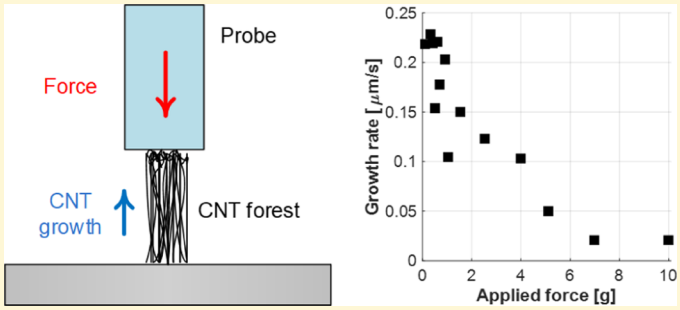

ABSTRACT: Ordered synthesis of one-dimensional nanostructures, such as carbon nanotubes (CNTs), involves competition between the growth kinetics of individual structures, their physical entanglement, and intermolecular forces that cause coupling of structures in close proximity. Specifically, CNT synthesis by chemical vapor deposition can directly produce films and fibers by providing CNT growth sites in close proximity such that the CNTs self-align into macroscopic assemblies. Because CNTs are mechanically coupled during these processes, the question arises as to whether or not mechanical forces intrinsic to the formation of CNT ensembles influence the growth kinetics and quality of CNTs, as can be expected from fundamental theories of mechanochemistry. Here, we study how mechanical forces influence CNT growth by applying controlled compression to CNT forests in situ; and relate the outcomes quantitatively to the CNT morphology and lengthening rate. We find that applied forces inhibit the self-organization of CNTs into a forest and accelerate the termination of collective growth. By correlating in situ kinetics measurements with spatial mapping of CNT orientation and density by X-ray scattering, we find that the average growth rate of individual CNTs is also mechanically modulated; specifically, a 100-fold increase in force causes a 4-fold decrease in average CNT lengthening rate. We attribute the slower growth kinetics to a stress-dependent increase of 0.02−0.16 eV in the effective activation energy for CNT growth. Via finite element modeling, we conclude that the force magnitudes that cause remodeling of the growing CNT network are less than the average strengths of adhesive contacts between CNTs. Last, we find that CNT growth rate and orientation can respond dynamically to changes in applied force, further demonstrating the mechanochemical nature of CNT growth and suggesting new approaches to control CNT quality and morphology in situ, with general application to other one-dimensional nanostructures.

INTRODUCTION

The influence of mechanical forces on chemical and structural transformations at the atomic scale is significant to materials processing in many contexts. For example, applied forces can

Received: August 27, 2018
Revised: December 13, 2018
Published: December 15, 2018

© 2018 American Chemical Society

DOI: 10.1021/acs.chemmater.8b03627
Chem. Mater. 2019, 31, 407−418

activate reversible conformational changes of individual polymer chains[1] and cause irreversible extension due to force-induced isomerization.[2] Mechanical strain can also alter the surface diffusion pathways of adatoms,[3] thereby influencing nucleation and growth of heteroepitaxial films.[4,5] In biological systems, mechanical forces have been shown to enhance the growth velocity of actin and neuronal networks.[6,7] In recent studies, it was also found that contact pressure increased the rate of antiwear tribofilm growth between a Si atomic force microscopy (AFM) tip coated with diamond-like carbon and a Fe-coated Si substrate,[8] and that mechanical agitation enhanced diffusion and reaction rates during the formation of elongated TiO_2-based nanotubular structures.[9]

For these reasons, it has been hypothesized that forces can be used to enhance control of carbon nanotube (CNT) synthesis, whose elongated geometry and interaction with other CNTs and/or substrates during synthesis causes the CNTs to experience entanglement, friction, and adhesive forces during elongation.[10] The hierarchical coupling of individual CNTs into a collective ensemble is intrinsic to formation of CNT aerogels, fibers, and sheets in the floating catalyst CNT method, and to the self-organization of CNTs into vertically aligned CNT "forests". For instance, in CNT forest growth, it is well-known that the individual CNTs within the forest do not grow uniformly; the distribution of sizes, orientations, and spacing of CNTs results in waviness of the CNTs,[11,12] and the distribution of lifetimes of the individual catalyst particles results in a significant density decay through the height of the forest from top to bottom.[11] Further, van der Waals (vdW) adhesion between CNTs that are in contact during growth gives rise to mechanical competition among CNTs, contributing to their tortuosity.[10,12−14] These intrinsic inhomogeneities influence the mechanical, thermal, and electrical properties of the CNT forest.[15−17]

Therefore, in order to advance understanding of CNT synthesis, it is important to learn how mechanical forces develop within CNT forests during growth, and how these forces influence the morphology and resulting properties of individual CNTs. Previously, Hart and Slocum demonstrated that requiring a growing CNT forest to lift a weight placed on the catalyst substrate reduces the terminal height of the forest, and that the alignment and structural quality of the CNTs are degraded by the applied pressure.[18] Further, the heterogeneous growth rates and orientations of CNTs within forests, combined with their mechanical coupling, cause forces to be transmitted to the CNT−catalyst interface. In previous work, we estimated that the strength of adhesion-induced coupling between CNTs, along with diameter-dependent differences in the growth rate, could impart a load ∼10 nN on a catalyst particle during growth.[13] Further, Han et al. developed a mechanochemical model of forest growth termination based on the observations of depressions in the top of the forest after growth. They hypothesized that CNT growth ceases when the intrinsic stresses create an energy barrier greater than the energy supplied during the CNT growth reaction, and the mechanical coupling among CNTs then creates a ripple effect leading to abrupt forest growth termination.[19] Additionally, Maschmann suggested, via simulations of growth of CNTs into a 2D array, that the wavy morphology of the CNT forests develops because of the disparate growth rates and CNT−CNT vdW coupling.[12] Nevertheless, there lacks a direct verification that forces influence the lengthening of CNTs, and how the mechanical remodeling of the CNT network (e.g., spatial changes in waviness and density), both relate to and can be decoupled from mechanochemical effects on the CNT formation process occurring at the catalyst particle.

In this paper, we utilize a custom chemical vapor deposition (CVD) system with a force-controlled manipulator to study the influence of mechanical forces on the morphology and growth dynamics of CNT forests. We apply compressive forces to millimeter-scale CNT forest pillars during growth, and find that applied forces can oppose the self-organization of the CNTs, and reduce the collective forest growth rate and lifetime. By combining these measurements of force-modulated growth kinetics with spatial X-ray mapping of the CNT morphology and density, we isolate and quantify how forces both modulate the CNT forest structure during growth, and slow the chemical process of CNT growth (lengthening). Using a three dimensional (3D) finite element model of load transmission through the forest, we find that the applied forces required to measurably perturb the growth are significantly less than the average intrinsic CNT−CNT contact strength within the forest, and result in a distribution of nanoscale loads at the CNT−substrate interface.

RESULTS AND DISCUSSION

A custom-built cold-wall CVD reactor with an integrated mechanical probe was used to apply controlled compressive loads to CNT forests during growth (Figure 1a,b). The probe is a fine quartz rod attached to a load cell and an electromagnetic linear actuator. A linear optical encoder was used to monitor the position of the probe, and the applied force was maintained via a feedback control system. Further details of the apparatus are in the Supporting Information.

In a typical experiment, the probe is placed in contact with the catalyst-coated substrate prior to heating. The force and displacement data are recorded in real time, and a camera provides a side view of the substrate−CNT-probe area (Figure 1c,d). A low load (0.1 g) is maintained as the substrate is heated and stabilizes while annealing in hydrogen and helium, and then the experiment load is set—increasing the contact force between probe and substrate—and the hydrocarbon feedstock (a mixture of ethylene and acetylene)[20] is introduced. During CNT growth, a constant setpoint load is maintained via feedback control of the probe position, by actuating the probe upward such that its position follows the upward displacement of the CNT forest. Once the probe stops moving, indicating that the forest growth has self-terminated, the gas is switched to helium and the system is cooled. In Figure 1e, we show the substrate temperature and CNT height trajectories for a typical experiment under constant compressive force.

Experiments were performed with patterned-catalyst substrates giving a circular CNT growth area of 1 mm diameter, which was aligned underneath the probe. Application of compressive loads from 0.1 to 10 g therefore resulted in an effective compressive stress ranging from 1.2 to 125 kPa on the CNT forest as it grew. At loads of less than 0.7 g, the height kinetics were determined to be unchanged by the applied load. For instance, forest height versus time under a constant compressive load of 0.3 g (4.0 kPa, based on the area of the CNT forest) is shown in Figure 2a. The vertical growth rate is calculated by numerical differentiation of the height versus time curve, also shown in Figure 2a (green line). During the initial stage of disorganized CNT growth, the probe position moves upward at 0.08 μm/s because of the thermal expansion of the system in the growth environment, as observed in the calibration

DOI: 10.1021/acs.chemmater.8b03627
Chem. Mater. 2019, 31, 407−418

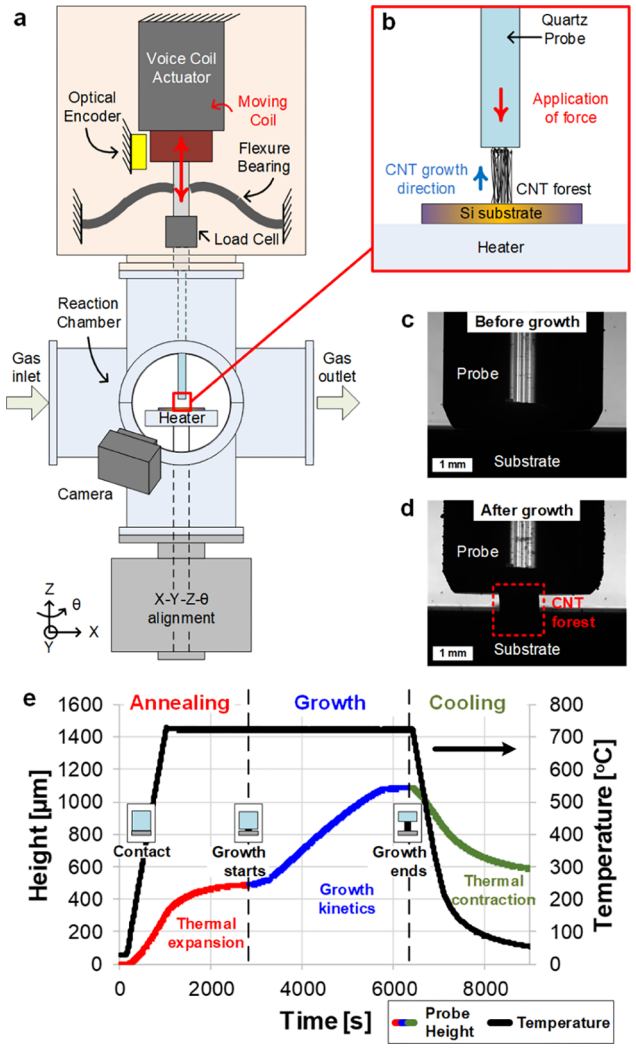

Figure 1. System and method for force-modulated CNT growth (a) schematic of system with voice coil linear actuator driving a vertical probe via load cell, with inset (b) showing application of force onto a growing forest with a cylindrical probe. Optical images of the reaction zone taken before (c) and after (d) growth of a 1 mm diameter CNT pillar. (e) Plot of probe displacement and temperature throughout an exemplary experiment. Thermal expansion occurs and stabilizes during the annealing stage, and the net upward displacement of the probe during the growth stage, while a steady force is maintained, represents the height of the CNT forest.

experiment that is detailed in Figure S2. After this, we measure a sharp increase in the growth rate to 0.19 μm/s, indicating that the forest has self-organized into vertical alignment;[10] we define the growth rate at this time, circled in red in Figure 2a, as the initial growth rate. The rate then increases to a maximum of 0.25 μm/s, and then slowly decays. Eventually, forest growth self-terminates, which is indicated by a rapid drop in the growth rate.[14]

By performing a series of force-controlled CNT growth experiments (Figure 2b) at constant compressive loads (0.1−10 g; 1.2−125 kPa), we observe that compressive forces can slow the vertical growth rate and lead to a shorter terminal forest height (Figure 2c). For instance, a forest grown under 0.1 g achieved approximately 1000 μm in height, whereas one grown under 10.0 g only reached 80 μm before self-termination. In these experiments, we find that growth self-terminates earlier at higher loads (Figure S3). We also compare the initial and average growth rates for each experiment, as shown in Figure 2d. The average growth rate is calculated for the duration starting immediately after the sharp rise in the growth rate, and ending with forest termination (which we define as when the growth rate is <10% of the maximum rate), as indicated by the arrow in Figure 2a. The average growth rate decreases with increasing applied load; thus, the applied load not only restricts the height that the forest can achieve, but also retards the growth of the forest once lift-off has occurred.

Self-termination of CNT forest growth by thermal CVD is often accompanied by a loss of CNT alignment at the base of the forest, because of gradual decay of the number density of growing CNTs until the CNTs can no longer remain self-aligned.[11,14] In force-controlled growth experiments, we observe an earlier loss of alignment, at a height inversely proportional to the compressive force applied (Figure S4). Moreover, beyond a critical force we find that the CNT forest is unable to self-organize and only grows slowly upward as a tangled ensemble.

As such, we can classify our results into three regimes according to the magnitude of applied force: (i) low loads of 0.1−0.6 g (1.2−7.5 kPa, over the area of the forest); (ii) moderate loads of 0.7−4 g (8.7−50 kPa); and (iii) high loads of 5.1−10 g (64−125 kPa). The characteristic features in the forest-height kinetics for the three regimes (Figure 3a) reflect changes in morphology observed in scanning electron microscope (SEM) images (Figure 3c−h). In regime (i), the forest has vertical alignment through its height (Figure 3c,d). However, a forest grown under a moderate force, after a period of growth with steady vertical alignment, transitions to a densified state in which the CNTs subsequently grow more tortuously (Figures 3e,f and S5). This transition is marked by a sudden drop in the measured vertical growth rate. In the high-force regime, the maximum growth rate is much lower, and SEM imaging reveals that the entire forest has a disordered, tangled morphology (Figure 3g,h). Growth under applied loads produces CNTs of low structural quality with kinks and deformations as demonstrated in transmission electron microscope (TEM) images (Figure S6); however, there is no clear indication that the magnitude of load influences the number of defects.

Next, small-angle X-ray scattering (SAXS) was used to map the orientation, diameter, and density of the CNTs within each forest, with a vertical spatial resolution of approximately 20 μm (see Methods). In Figure 3b we show Hermans orientation values (f) obtained from SAXS data. The Hermans parameter provides a spatially resolved measure of the CNT alignment: f = 1 denotes perfect vertical alignment, f = 0 denotes random orientation, and f = −0.5 denotes horizontal alignment. The forests that self-organize reach a maximum orientation (f = 0.3−0.4) within the first 100 μm of growth, and then orientation decreases gradually, and then collapses (f becomes negative) suddenly at a height that is inversely proportional to the magnitude of the applied force. At the highest applied loads (>5 g), the initially random orientation ($f \approx 0$) further decays with time as the CNTs grow laterally to evade the forced constraint. The mass density, which is generally proportional to the number of CNTs at each vertical position, is calculated from the Porod invariant[21] using the integrated scattered intensity (Figure 4; see Methods). The local mass density increases during self-organization, then decays gradually, then increases abruptly upon collapse; to the best of our knowledge, this is the first observation of an increase in forest density at termination. In general, we find that higher forces result in forests with greater

DOI: 10.1021/acs.chemmater.8b03627
Chem. Mater. 2019, 31, 407−418

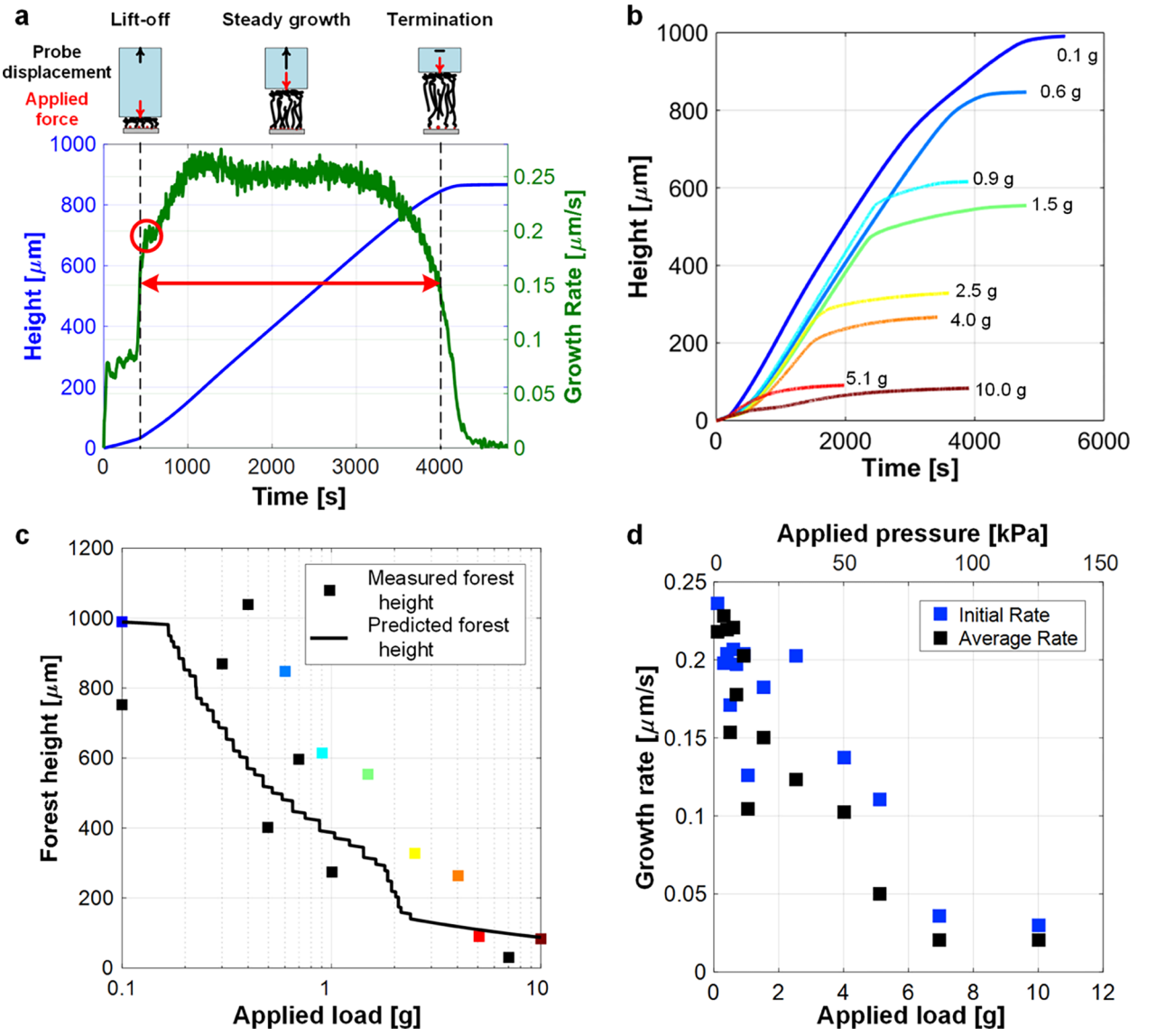

Figure 2. (a) Measured CNT forest height (blue) and the corresponding calculated growth rate (green) vs time during a nominal experiment under 0.3 g compressive load. (b) Height vs time curves for experiments with compressive loads ranging from 0.1 to 10.0 g. (c) Comparison between measured (points) and predicted (line) terminal heights vs applied load, using the height data measured in situ and the mechanical model presented in the text. The colored points correspond to the experiments in (b). (d) Initial and average growth rates measured from height vs time data, plotted vs applied load.

average mass density due to mechanical densification during constrained growth, yet the mass density must be decoupled from the CNT diameter and orientation in order to elucidate force-mediated changes in individual CNT growth kinetics.

At this point, we must resolve the difference between *mechanical* and *mechanochemical* responses to the applied load during CNT forest growth. In other words, we must decouple changes to the collective forest growth kinetics due to deformation of the forest (i.e. *mechanical* effects), from the possible force-modulation of the kinetics of individual CNT growth (i.e. *mechanochemical* effects). During growth under compression, the stress applied by the probe is transmitted through the forest to the base where the catalyst particles act to lengthen the CNTs, and we expect some elastic compression of the forest as well as possible CNT deformation at the catalyst interface. In what follows, we show that we primarily observe macroscopic mechanical effects when we look at the collective forest kinetics, but we also see evidence of mechanochemical effects when we calculate true CNT lengthening kinetics.

First, we find that the accelerated collapse of CNT forests during force-retarded growth is purely a mechanical effect due to collective buckling of the CNTs at the base, as observed in a typical mechanical compression test of a CNT forest.[22,23] We develop a model of the CNT forest as a foam-like material, for which the properties are dependent on volume fraction ϕ of the constituent fibers, and thus vary along the forest height. The forest modulus is estimated as (see Methods for details)[24]

$$E^* = E_{CNT}\phi^2 \quad (1)$$

where E_{CNT} is the elastic modulus of a single CNT, taken to be 1000 GPa.[25] We consider the forest to initially have undergone a phase transition to a densified state at the point of collapse.[26] Assuming that the forest behaves like an open-cell foam, the collapse stress is proportional to the elastic modulus of the forest

DOI: 10.1021/acs.chemmater.8b03627
Chem. Mater. 2019, 31, 407−418

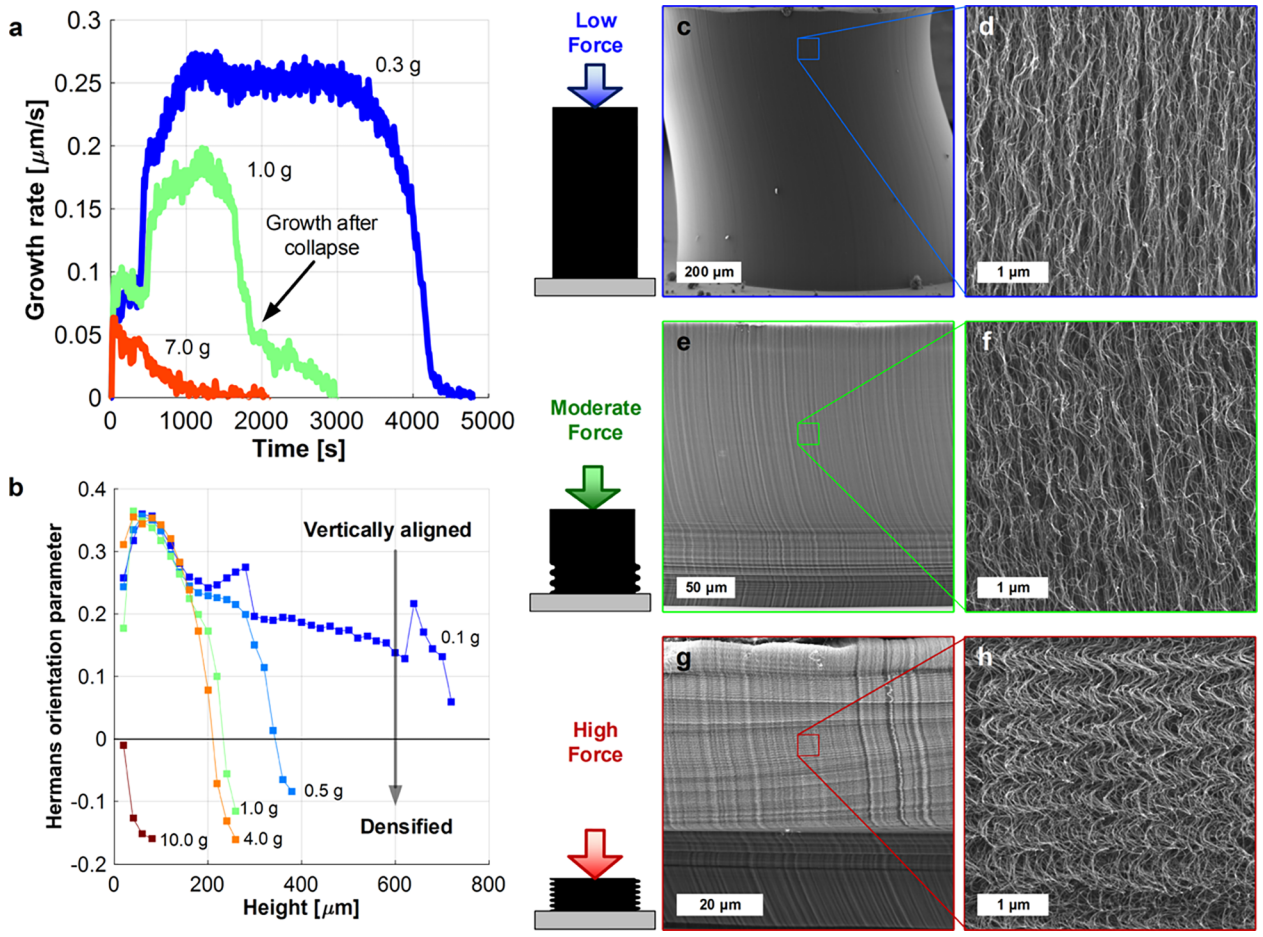

Figure 3. (a) Rate of CNT height increase from experiments at low (0.3 g), moderate (1.0 g), and high (7.0 g) applied loads. The arrow indicates the lower growth rate after collapse of the forest under moderate force. (b) Hermans orientation parameter, determined by SAXS, indicating alignment of CNTs throughout each forest (height = 0 represents the top). The sharp drop in the orientation value to below 0 marks the densification of the forests. (c,e,g) SEM images of forest sidewalls from experiments at low, moderate, and high applied forces, and (d,f,h) respective higher magnification images showing local morphology.

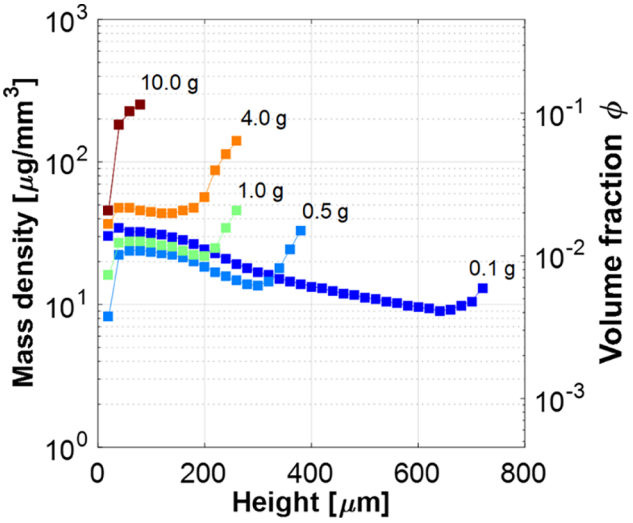

Figure 4. Mass density and equivalent volume fraction profiles, as determined by SAXS. Height 0 is the top of the forest.

(see Methods). Therefore, we can estimate the stress to cause collapse for a given volume fraction from the measured collapse stress ($\sigma_{c,measured}$) and elastic modulus ($E_{l,measured}$) from a high-temperature compression test (Figure S7)

$$\sigma_c^*(\phi) = \sigma_{c,measured}\frac{E^*(\phi)}{E_{l,measured}} \quad (2)$$

Before collapse, the forest is a linear elastic foam. After collapse, the forest is modeled with a power-law stress−strain relationship as developed by van-Wyk and Toll for densely-packed fibers.[27,28]

A nominal forest of height 1000 μm (the case of $\sigma_{applied} = 0$) is discretized into horizontal "slices"; a profile of volume fraction versus height for the forest obtained by SAXS is used to assign a volume fraction ϕ_i to each slice. The resulting strain at each vertical location is therefore

$$\varepsilon_i = \begin{cases} \dfrac{\sigma_{applied}E_i^*}{} & \sigma_{applied} < \sigma_c(\phi_i) \\ 1 - \left(1 + \dfrac{\sigma_{applied}}{kE_{CNT}\phi_i^3}\right)^{-1/3} & \sigma_{applied} \geq \sigma_c(\phi_i) \end{cases} \quad (3)$$

where k is an empirical constant to account for geometry of fiber segments, here taken to be unity. Finally, the predicted height H of the forest after compression is found by summing the compressed heights of each forest slice

DOI: 10.1021/acs.chemmater.8b03627
Chem. Mater. 2019, 31, 407−418

$$H = \sum_{i}^{N} h(1 - \varepsilon_i) \quad (4)$$

Via this approach, the CNT forest height is accurately predicted (Figure 2c) according to its measured, spatially-varying morphology, including the force-mediated collapse whereby the base of the forest transitions from the vertically-oriented to tangled morphology. Additionally, mechanical compression tests of CNT forests after growth (Figure S7) show that the critical stress to induce the phase transition is comparable both during and after growth. Therefore, we conclude that the in situ collapse of CNT morphology is mechanically mediated rather than a coupled mechanochemical process.

Mechanochemical effects may still be present, but are obscured by variations in density, diameter, and tortuosity of the CNT population. Hence, to elucidate possible mechanochemical effects we must determine the lengthening rates of individual CNTs. CNTs are approximated to have a sinusoidal shape (as evidenced by SEM images in Figure 3) with a waviness that is dependent on the locally measured orientation parameter; in combination with the real-time forest growth kinetics, we therefore obtain the CNT lengthening rate versus the applied load (see Figure 5 and Methods). As shown in Figure 5c, the average CNT lengthening rate decreases with increasing load, even though the average length of a CNT relative to the forest height increases with load (Figure S8). Therefore, after accounting for the tortuosity of the CNTs arising due to the force-induced change in their alignment, we conclude the CNTs lengthen more slowly due to the opposing, externally applied load. Additionally, our analysis suggests that smaller diameter CNTs are more prevalent at higher applied loads and as growth proceeds to termination (Figure S9). The precise force-dependent kinetics will depend on the force applied to each CNT at the base, which certainly varies according to its diameter and orientation.[13,29] Nevertheless, we estimate the average force acting on each CNT ranges from around 10 pN to 1 nN over the areal number density range of 7×10^8 to 2×10^{10} CNTs/cm^2 (Figures 6a and S10) representative for the series of experiments in this study.

The estimated number density of CNTs in the forest is found to be about 10× greater at the highest load compared to the lowest load (Figure S10a). We can attribute this to several factors. First, the load compresses the forest such that CNTs form an entangled ensemble, and additional CNTs that nucleate later during the growth process become included in this ensemble and overwhelm the decreasing number density of CNTs that are still growing. This contrasts with an aligned forest, where additional CNT nucleation during growth is balanced by decay as the forest moves upward. Second, in our X-ray analysis we assume that each CNT can be projected onto a plane without self-intersection, whereas a particularly long and tortuous CNT that partly extends in the direction of the X-ray beam during measurement might be double-counted. Third, we cannot rule out changes in the particle density and/or the catalyst activity, either directly or indirectly as a result of the applied load. The average CNT diameter is smaller at higher load (Figure S9a), suggesting there may be more catalyst particles at higher loads, contributing to the greater number density. Nevertheless, in spite of these uncertainties, our analysis demonstrates that force modulates the lengthening rate of

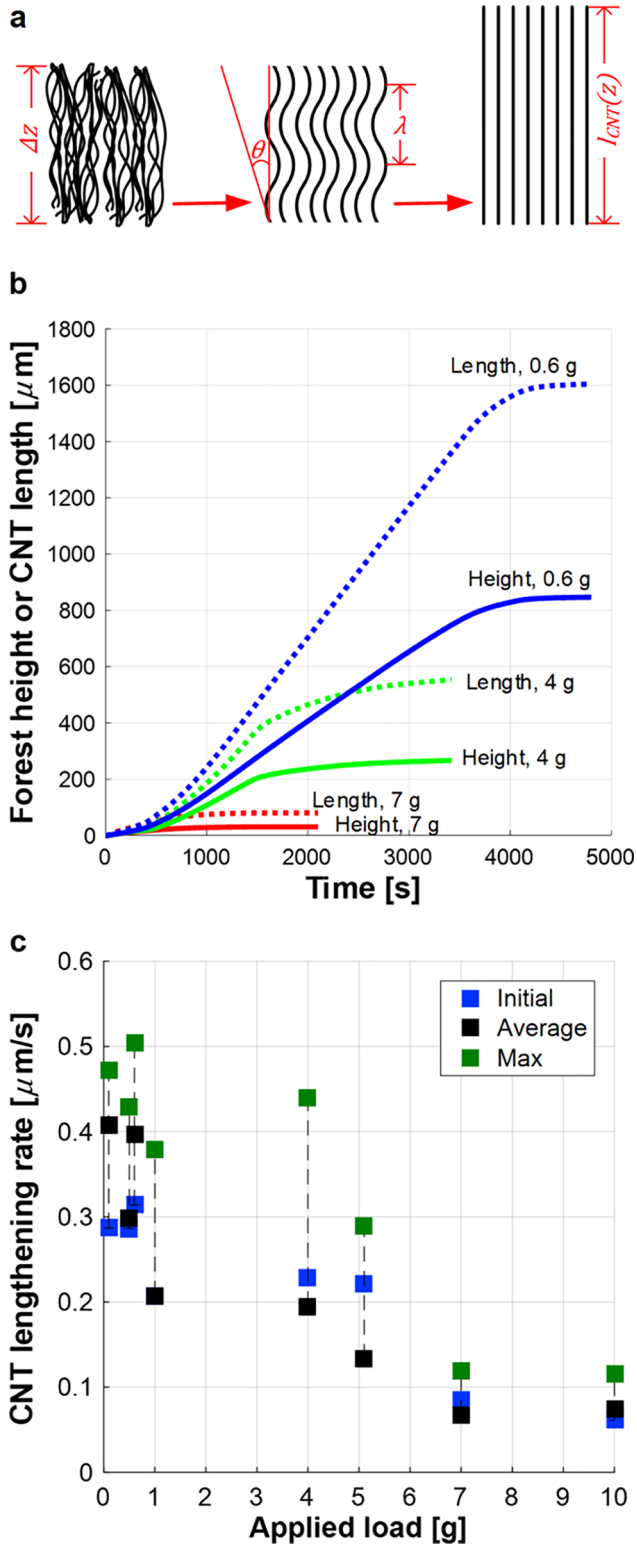

Figure 5. (a) Schematic showing the determination of the effective CNT length corresponding to each forest height. (b) Forest height and CNT length vs growth time for representative forests grown under different applied loads. (c) Initial, average, and maximum lengthening rate of a representative CNT throughout growths under load.

CNTs, which is a direct measure of the mass output of the CNT growth reaction versus time.

The observed inverse relationship between CNT lengthening rate and load applied to the CNT forest implies that mechanical

DOI: 10.1021/acs.chemmater.8b03627
Chem. Mater. 2019, 31, 407−418

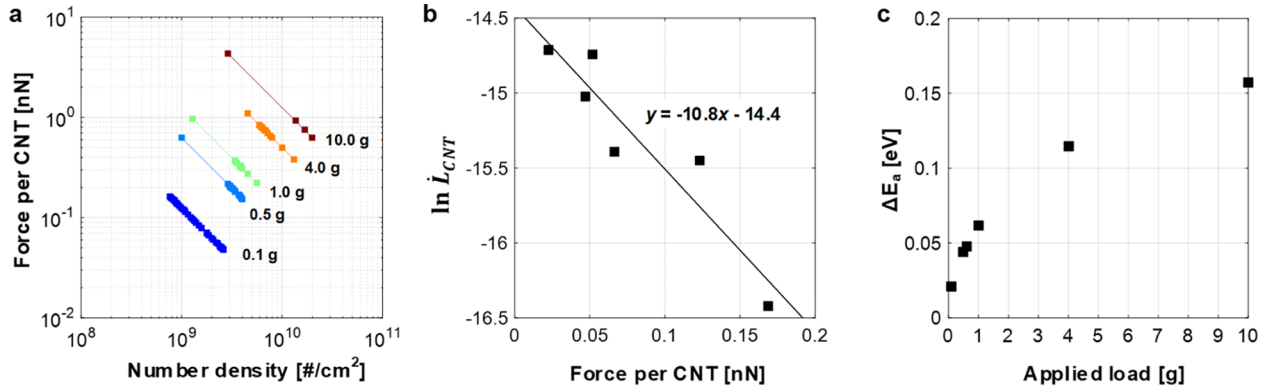

Figure 6. Mechanical force alters the effective activation energy of CNT growth: (a) estimated average force applied at the base of each CNT, across the range of number densities determined by SAXS for each experiment. (b) Log-linear fit of CNT lengthening rate with average applied force per CNT, showing an Arrhenius-like relation from which the reaction coordinate α is approximated by a linear fit. (c) Apparent shift in activation energy ΔE_a versus applied load.

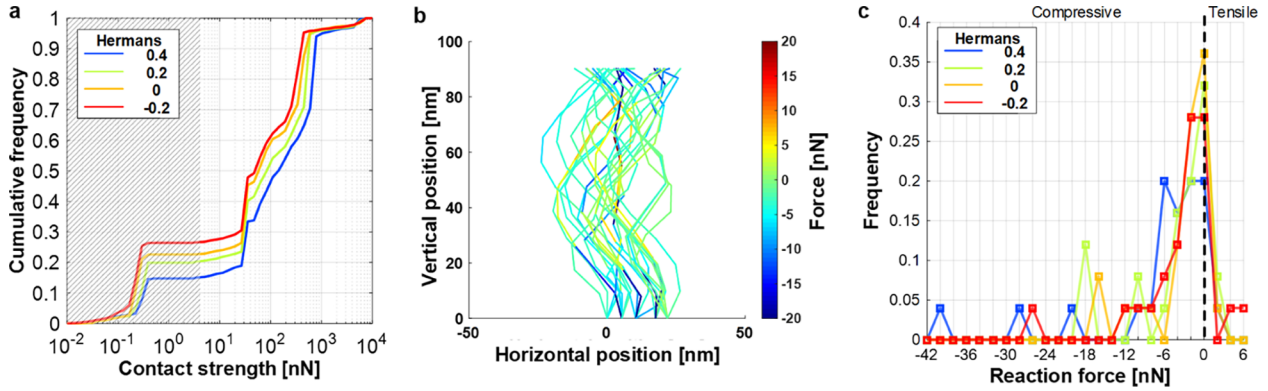

Figure 7. (a) Calculated cumulative distribution of contact strengths for CNT forests having noted orientation values. The shaded region of the plot indicates the range of per-CNT forces applied in our experiments. (b) Axial force distribution within a simulated 5 × 5 CNT array (initial orientation parameter = 0.4) after compression to 10% strain, and (c) corresponding calculated distribution of reaction forces at the bases of the CNTs after simulated compression, including that for forest models of different orientation values.

stress at the catalyst causes an increase in the effective activation energy (ΔE_a) for CNT growth. Previous studies of CNT forest synthesis by thermal CVD using Fe catalyst have found an effective activation energy for CNT growth in the range of 1.02−2.0 eV, by fitting growth rate data at various temperatures using the Arrhenius method.[30−33] For growth under mechanical load, we consider an Arrhenius-like dependence, such that the lengthening rate $\dot{L}_{CNT}$ of a representative CNT is proportional to $e^{-(E_a+\Delta E_a)/kT}$, independent of the CNT length. Here, E_a is the effective activation energy of CNT growth under no mechanical load (which we assume to be constant for our experiments), k is the Boltzmann constant, and T is temperature. We express $\Delta E_a = \alpha\sigma$, the reaction coordinate (α) multiplied by the average applied force per CNT (σ). The applied force per CNT is approximated as the total force applied to the forest divided by the average number density, which is measured by SAXS. Thus, we can form an Arrhenius-like mathematical formulation for a force-dependent growth rate of CNTs, wherein stress is varied rather than temperature

$$\ln \dot{L}_{CNT} = \frac{\alpha}{kT}\sigma + C \tag{5}$$

The constant C captures all terms independent of stress. Plotting $\ln \dot{L}_{CNT}$ versus σ and taking a linear fit (Figure 6b), we approximate α = 0.15 nm; this value is close to the length of a carbon−carbon bond in a CNT (0.142 nm),[34] suggesting that the load influences the rate of carbon addition at the CNT−catalyst interface.

After determining α, ΔE_a can be determined for each applied load (Figure 6c). We calculate a monotonic increase in the stress-dependent ΔE_a, ranging from 0.02 to 0.16 eV, for 0.1−10 g of applied load, respectively. This indicates that perturbations in the effective activation energy measurably influence the CNT growth rate; the mechanical force is altering the energy barrier for construction of the CNTs, and the energy barrier increases with applied compressive force. We cannot ascertain the extent to which the force precisely influences rate as well as quality (i.e. probability of defects in individual CNTs), but the higher effective activation energy reduces the rate of bond formation under otherwise fixed growth conditions. Future investigation of the dependence on temperature and reaction conditions will enable more comprehensive understanding of force-mediated growth kinetics.

Transmission of load through the growing forest, and to each catalyst particle at the base, is also influenced by the adhesive interactions between contacting CNTs. We therefore compare the per-CNT forces shown to influence growth with the strengths of CNT−CNT contacts within the forest. The contact strength between any pair of CNTs within the forest is determined by the local contact area that results from a balance between elastic deformation and vdW adhesion, which is determined by the diameter, wall number, and shape of each

DOI: 10.1021/acs.chemmater.8b03627
Chem. Mater. 2019, 31, 407−418

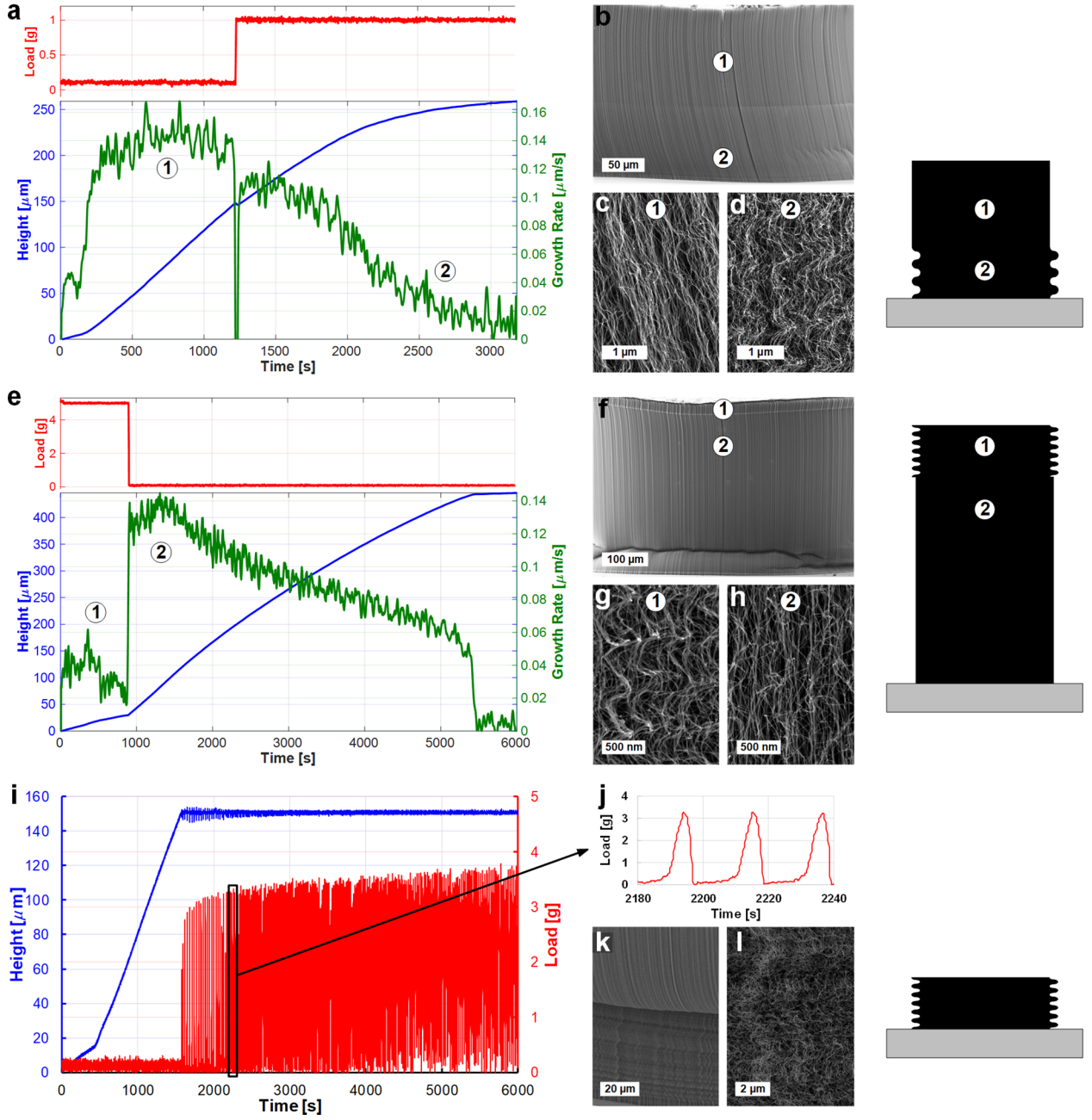

Figure 8. Applied compressive load, forest height, and growth kinetics throughout a growth for a dynamic load application in which (a)load was increased to 1 g after 150 μm of growth under 0.1 g compression, and (e) load was relieved to 0.1 g after 15 min of growth under 5 g compression. (i) Height and load trajectories for a growth under 0.1 g compression to 150 μm, at which point the probe was held at a fixed position while growth continued. (j) Measured load for the 10th min after the probe was commanded to maintain a fixed position. (b,f,k) SEM images of forest sidewalls and (c,d,g,h,l) higher magnification images of the regions under different loads.

CNT.[35] Using a three-dimensional model of the wavy morphology of the CNT forest and analytical calculation of the strength of each contact,[35] we derive the distribution of contact strengths (Figure 7a) for CNT forests with alignments spanning the range in the force-modulated growth series. We find that the contact strength distribution shifts upward with greater vertical alignment of CNTs, because the alignment induces a greater contact area between CNTs. The model predicts the applied forces per CNT are not sufficient to overcome the CNT−CNT contact strength at low applied forces, yet are likely greater than some of the contact strength values for experiments with high applied forces. This is consistent with our observations that lower forces do not remodel the CNT forest until the density is low due to decay during growth, yet higher forces prevent self-organization.

Further, because the applied force is distributed through the CNT network, the bases of the CNTs feel forces that are proportional to the applied force, albeit distributed over a wide range. A finite element model of the compression of a representative forest segment, with CNT−CNT contact strengths determined as mentioned above, predicts the force distribution through the forest segment (Figure 7b) and the reaction forces at the CNT bases (Figure 7c), ranging from compressive to tensile. However, note that the magnitude of

DOI: 10.1021/acs.chemmater.8b03627
Chem. Mater. 2019, 31, 407−418

forces in this simulation do not necessarily correspond to those experienced during growth because a strain rather than a stress is applied during the simulation, and the simulated array of limited height and number of CNTs might not fully capture the complex interactions within a full forest.

The present study is the first to show that forces can modulate the growth rate of CNTs. The prior knowledge of intrinsic force development during growth without applied force suggests that CNT forest growth kinetics—and perhaps quality—are mechanically as well as chemically mediated. The model of Han et al. mentioned in the introduction to the paper incorporates mechanical coupling of CNTs and considers the mechanochemical consequences to growth, specifically a catastrophic termination of forest growth once intrinsic stresses reach a critical limit.[19] However, due to the gradual CNT density decay until collapse of the forest, we find that the stresses at the catalyst serve to continually mediate CNT growth rather than solely provide an abrupt termination mechanism. Our findings are also supported by two-dimensional CNT array simulations of growth and compression, showing that stresses develop due to the disparity in CNT size and the CNT−CNT mechanical couplings (which are maintained throughout growth),[12] but we prescribe a three-dimensional wavy morphology of CNTs to match the characteristics of our forests grown under load and mark the variation in forces that develop at the catalyst growth front. Additionally, the intrinsic forces exerted by growing CNTs span a distribution because of the various orientations and contact conditions of CNTs at the base of the forest.[10,13] Applying an external force will bias this force distribution, while retaining a distribution of forces that collectively slow the forest growth rate and lead to remodeling of the network, which is proven by the collapse at a critical stress as the density decays.

We have also found that the rate of CNT growth responds to programmed changes in applied load, further validating that applied force may be used to spatially tailor CNT morphology during growth. Starting CNT growth under low load (0.1 g) and then increasing to a higher load (1 g) causes a decrease in the forest growth rate and an increase in CNT tortuosity (Figure 8a−d). Conversely, starting at a high load (5 g) and decreasing to a lower load (0.1 g) causes an increase in the forest growth rate and enhanced vertical alignment (Figure 8e−h). As a final example, a CNT forest is grown under 0.1 g to a height of 150 μm, at which point the probe is commanded to hold a fixed position (Figure 8i−l); the periodic spikes in the measured load upon further growth (e.g. Figure 8j) illustrate the dynamic load transmission and morphological rearrangements of a growing forest. Thus, we expect that time-varying external forces could, for example, be used to construct CNT forests with spatially tailored alignment and resulting variations in mechanical, thermal, or other properties.

CONCLUSIONS

In summary, we find that externally applied mechanical forces influence CNT forest growth, by affecting the self-organization, growth rate, and termination behavior. Combining in situ measurements of CNT forest height under a range of forces with quantitative X-ray analysis, we are able to decouple mechanical effects of forces on CNT morphology from mechanochemical effects in which the forces exerted upon the CNT−substrate interface cause an increase in the effective activation energy for CNT growth such that CNT lengthening slows. Our findings motivate further investigation of the underlying mechanisms by which CNT growth is mechanochemically controlled, as well as the development of new CNT growth instruments that may apply directed forces to influence CNT self-organization, lengthening, and assembly during the CVD process. Further insights could be gained by applying mechanical forces on individual growing CNTs such as using micro-manipulation in combination with environmental TEM. Further, application of different stress states (e.g. shear or tensile stresses) during growth could reveal additional morphological and mechano-chemical responses, such as the possibility to enhance CNT growth rate and quality by applied tension.

METHODS

Catalyst Preparation. To prepare samples for CNT growth, a 4″ (100) Si wafer with 300 nm of a thermally grown oxide layer is patterned with 1 mm diameter circles using standard photolithography techniques and positive resist SPR 700. Then, Al_2O_3 and Fe catalyst layers of thickness 10 and 1 nm, respectively, are deposited by electron-beam evaporation. The wafer is then diced with a dicing saw into samples of size 1 cm × 1 cm, with a single patterned catalyst circle in the center of each sample. The patterned samples require a lift-off procedure to remove the photoresist before conducting an experiment, by placing the sample in a beaker of acetone and into an ultrasonic bath, repeated with fresh acetone and then rinsed with isopropanol and dried with a stream of N_2 gas. The Fe layer dewets into catalyst nanoparticles during the annealing stage of an experiment.

CNT Growth. Before each experiment, the CVD system is baked out by heating the closed system to 900 °C for 20 min to burn away carbon deposits remaining in the system. Then a sample is loaded onto the heater assembly and aligned with the $X-Y-Z-\theta$ positioning system so that it is centered under the probe. The chamber is sealed and pumped down to 100 mTorr to purge the system of contaminants. After flushing the system with He, the system is ready for growth. A custom LabVIEW program is then used to bring the probe down to touch and maintain contact with the sample surface at 0.1 g compression, and to implement a heating and gas flow recipe as described in Table S1. Just before the hydrocarbon gases are introduced to start growth, the applied load is switched to the desired amount. The probe must maintain contact with the sample throughout the experiment in order to register height change of the heater stage during thermal expansion, to cover the catalyst during the annealing step in order to prevent excessive heat dissipation in the cold-wall system so that the catalyst particles properly form, and to measure the growth of the forest. The growth is also monitored in situ with a digital camera. When the CNT forest has finished growing, the growth step is ended and the system is cooled down to below 50 °C, at which point the probe is slowly moved upwards away from the forest at a rate of 1 μ/s.

Upon completion of an experiment, the measured probe displacement during the growth step is extracted to obtain the forest height during growth. The height is then numerically differentiated between successive points with respect to time to obtain the growth rate versus time. A moving average filter is used to remove high frequency random noise in the growth rate and to obtain the rate as seen in Figures 2 and 3.

SAXS Analysis. SAXS characterization was performed at the 12-ID-B beamline at the Argonne National Lab Advanced Photon Source. Two-dimensional SAXS intensity maps, captured with a Pilatus 2 M pixel detector, were obtained by passing the 14 keV X-ray beam confined to 15 μm vertically through the thickness of a forest, and scanning the beam through the forest from top to bottom at 20 μm increments. The measured intensities are converted to absolute values in cm^{-1} at the beamline using a glassy carbon calibration sample. The amount of vertical alignment of the CNTs at each probed forest segment is quantitatively analyzed by comparing the Hermans orientation parameter f as calculated from the average orientation angle θ obtained by azimuthal integration of the SAXS intensity I.[36]

$$f = \frac{1}{2}(3\cos^2\theta - 1) \tag{6}$$

DOI: 10.1021/acs.chemmater.8b03627
Chem. Mater. 2019, 31, 407−418

$$\cos^2\theta = \frac{\int_0^{\pi/2}(I(\theta)\sin\theta\cos^2\theta)\mathrm{d}\theta}{\int_0^{\pi/2}((I(\theta)\sin\theta)\mathrm{d}\theta)} \tag{7}$$

Next, the volume fraction of each forest segment is obtained by utilizing the Porod invariant Q from SAXS theory,[21] with the assumption that CNTs can be treated as azimuthally distributed infinitely long cylinders. Q is determined from the SAXS intensity map.

$$Q = \frac{1}{2\pi}\int_0^\infty q^2 I(q)\mathrm{d}q \tag{8}$$

where q is the scattering vector length, and $I(q)$ is the azimuthally averaged absolute scattering intensity. The volume fraction of CNTs is then determined from

$$Q = \phi(1-\phi)(\Delta\rho)^2 \tag{9}$$

Here, $\Delta\rho$ is the difference in scattering electron density between carbon and air, analytically determined to be 1.86×10^{15} m^{-2}. The Porod invariant was similarly used, for example, in studying the growth of gold nanoparticles[37] and of amorphous calcium carbonate particles.[38] The mass density of CNTs in a segment of the forest is then

$$\rho_\mathrm{m} = \rho_\mathrm{g}\phi \tag{10}$$

where ρ_g is the mass density of graphite, 2.2 g/cm^3. The forests grown were too small for the mass to be obtained with a microbalance.

The shape of an individual CNT is then approximated as a 3-dimensional sinusoid, parameterized in Cartesian space with

$$r = \left[A\sin\left(\frac{2\pi}{\lambda}z\right),\ A\sin\left(\frac{2\pi}{\lambda}z\right),\ z\right] \tag{11}$$

z is the distance in the axial direction, A is the amplitude, and λ is the wavelength. By estimating A = 30 nm from SEM images, λ can then be found from the average orientation angle θ obtained by above

$$\lambda = \frac{4A}{\tan\theta} \tag{12}$$

Thus, a representative shape of a CNT within the population and its length $L_\mathrm{CNT}(z)$ in a given forest slice of height Δz can be determined. By mapping the SAXS orientation angles along the forest height to the in situ growth kinetics measurements (Figure 2), the instantaneous CNT lengthening rate at time t is determined by

$$\dot{L}_\mathrm{CNT}(t) = \frac{L_\mathrm{CNT}(z)}{\Delta z}\cdot\dot{h}(t) \tag{13}$$

where $\dot{h}(t)$ is the instantaneous forest growth rate at that time. Additionally, the average total length of a CNT in a forest is

$$L_\mathrm{CNT} = \sum \dot{L}_\mathrm{CNT}(t)\cdot t \tag{14}$$

Further characterization of the CNT population within each forest slice is performed by fitting the I versus q curves with a scattering profile based on modeling the CNTs as hollow cylinders as in our previous work.[11] Here, assuming the CNT population has a log-normal distribution of outer diameters, we can determine the mode of the diameter distribution D_o, diameteral ratio c (inner diameter/outer diameter), and average number of walls. Then, the average volume of a CNT within a forest slice is

$$V_\mathrm{CNT} = L_\mathrm{CNT}\frac{\pi}{4}(1-c^2)\sum D_\mathrm{o}^2 P(D_\mathrm{o}) \tag{15}$$

Because the log-normal distribution is nonsymmetric, the diameters are divided into bins of width 0.5 nm. The square of each bin diameter is multiplied by the log-normal probability $P(D_\mathrm{o})$ of that diameter being represented in the population, and the results are summed to achieve a more accurate squared diameter than using the mode diameter to compute the average CNT volume. The average CNT volume is then used to calculate the areal number density for that forest slice

$$\rho_\mathrm{n} = \frac{\phi b}{V_\mathrm{CNT}} \tag{16}$$

where b is the beam height of 15 μm.

Finally, the average applied force per CNT is

$$F_\mathrm{CNT} = \frac{P}{\rho_\mathrm{n}} \tag{17}$$

where P is the pressure applied to the forest during growth.

Mechanical Modeling. First, we relate the volume fraction from SAXS to determine the elastic modulus of the forest. The CNT forest modulus E^* can be estimated from Gibson and Ashby[24]

$$E^* \approx E_\mathrm{CNT}\left(\frac{\rho^*}{\rho_\mathrm{CNT}}\right)^2 \tag{18}$$

Here, E_CNT is the elastic modulus of a single CNT, ρ^* is the density of the forest, and ρ_CNT is the density of a single CNT. If we equate the volume fraction to the relative densities $\phi = (\rho^*/\rho_\mathrm{CNT})$, we can approximate the CNT forest modulus as $E^* \approx E_\mathrm{CNT}\phi^2$.

To obtain a volume fraction-dependent modulus, we scale the volume fraction from SAXS appropriately with factor B by equating the measured modulus E_l from our high-temperature compression test with the average modulus E^* determined in N slices of equal height h that vertically span a nominal forest

$$E_\mathrm{l,measured} = \frac{1}{N}\sum_i^N E_\mathrm{CNT}(B\phi_i)^2 \tag{19}$$

Gibson and Ashby define for an open-cell foam

$$\frac{\sigma_\mathrm{c}^*}{E_\mathrm{CNT}} = C\left(\frac{\rho^*}{\rho_\mathrm{CNT}}\right)^2 \tag{20}$$

for a constant C that includes all constants of proportionality. Here, rearranging and using the previous expressions, the elastic collapse stress is found to be proportional to the forest modulus

$$\frac{\sigma_\mathrm{c}^*}{E^*} = C \tag{21}$$

We can then determine the elastic collapse stress for a forest of a certain volume fraction using the collapse stress $\sigma_\mathrm{c,measured}$ and elastic modulus $E_\mathrm{l,measured}$ measured in a compression test

$$\frac{\sigma_\mathrm{c}^*}{E^*} = \frac{\sigma_\mathrm{c,measured}}{E_\mathrm{l,measured}} \tag{22}$$

Imaging. SEM images were taken with a Zeiss Ultra55 field emission SEM (FESEM) and a Zeiss Supra55VP FESEM, and TEM images were taken with a JEOL 2100 TEM, at the Center for Nanoscale Systems at Harvard University.

Finite Element Modeling. A 3D finite element model of a forest section is generated with a MATLAB code that calculates the strength of contacts between CNTs. Each forest section has CNTs with sinusoidal geometries represented by nodes and constructed so that the section has the specified Hermans orientation value. The code searches for nodes that are within distance of 0.6 nm to determine contact locations, and the contact strength is found by considering the vdW attraction forces (approximated as hollow cylinder surface potentials) in the normal direction, and by the shear strength of CNTs in the transverse direction. The contact strength distribution was determined for an array 100 nm tall of 10 × 10 CNTs. Compression simulations were performed on an array 100 nm tall of 5 × 5 CNTs by inputting the CNT geometry and contact information into ANSYS finite element simulation software, which performed compressive displacements from the top of the array in 0.2 nm increments. This model is an adaption of a model we developed to simulate CNT yarns, and further details can be found in ref 35.

DOI: 10.1021/acs.chemmater.8b03627
Chem. Mater. 2019, 31, 407−418

■ ASSOCIATED CONTENT

Supporting Information

The Supporting Information is available free of charge on the ACS Publications website at DOI: 10.1021/acs.chemmater.8b03627.

Details of the custom CVD system for in situ load application, including a typical gas and temperature recipe, and probe height and load curves for a calibration experiment without CNT growth; results of time to lift-off, time to termination, and height at collapse of CNT forests grown under loads; SEM images of the forest sidewall at different vertical positions for a forest grown under moderate load; TEM images of CNTs grown under applied load; details of compression tests performed in the custom CVD system on pregrown CNT forests; additional details on CNT length versus applied load; properties of the CNT forest population (e.g. diameter, number of walls, number density) grown under load as a function of forest height, determined by SAXS (PDF)

In situ video (512× speed) of the growth of a CNT forest under a mechanical load in the custom-built CVD system (AVI)

Simulations of compression of a 5 × 5 CNT array to 10% strain, with varying initial orientation values of 0.4 (AVI), 0.2 (AVI), 0 (AVI), and −0.2 (AVI), corresponding to the data presented in Figure 7b,c

■ AUTHOR INFORMATION

Corresponding Author

*E-mail: ajhart@mit.edu.

ORCID

Nicholas T. Dee: 0000-0002-8633-3564
Mostafa Bedewy: 0000-0003-4182-7533
Byeongdu Lee: 0000-0003-2514-8805
Eric R. Meshot: 0000-0002-7951-6696
Piran R. Kidambi: 0000-0003-1546-5014
A. John Hart: 0000-0002-7372-3512

Notes

The authors declare no competing financial interest.

■ ACKNOWLEDGMENTS

We thank D. Copic and C. R. Oliver for assistance in building and testing the force-controlled CNT growth apparatus, originally at the University of Michigan. This research was supported by the Department of Energy, Office of Science (DE-SC0010795), and by the National Science Foundation Graduate Research Fellowship under grant no. 1122374 (to N.T.D.). SEM and TEM imaging was performed at Harvard University's Center for Nanoscale Systems (CNS), a member of the National Nanotechnology Infrastructure Network (NNIN), which is supported by the National Science Foundation under NSF award no. ECS-0335765. Catalyst patterning and deposition was performed at Microsystems Technology Laboratories (MTL) at MIT. SAXS characterization was performed at the 12-ID-B beamline at the Advanced Photon Source, a U.S. Department of Energy (DOE) Office of Science User Facility operated for the DOE Office of Science by Argonne National Laboratory under contract no. DE-AC02-06CH11357.

■ REFERENCES

(1) Rief, M.; Oesterhelt, F.; Heymann, B.; Gaub, H. E. Single Molecule Force Spectroscopy on Polysaccharides by Atomic Force Microscopy. *Science* **1997**, *275*, 1295−1297.

(2) Wu, D.; Lenhardt, J. M.; Black, A. L.; Akhremitchev, B. B.; Craig, S. L. Molecular Stress Relief through a Force-Induced Irreversible Extension in Polymer Contour Length. *J. Am. Chem. Soc.* **2010**, *132*, 15936−15938.

(3) Shu, D. J.; Liu, F.; Gong, X. G. Simple Generic Method for Predicting the Effect of Strain on Surface Diffusion. *Phys. Rev. B: Condens. Matter Mater. Phys.* **2001**, *64*, 245410.

(4) Brune, H.; Bromann, K.; Roder, H.; Kern, K.; Jacobsen, J.; Stoltze, P.; Jacobsen, K.; Norskov, J. Effect of Strain on Surface Diffusion and Nucleation. *Phys. Rev. B: Condens. Matter Mater. Phys.* **1995**, *52*, 14380−14383.

(5) Huang, L.; Liu, F.; Lu, G. H.; Gong, X. G. Surface Mobility Difference between Si and Ge and Its Effect on Growth of SiGe Alloy Films and Islands. *Phys. Rev. Lett.* **2006**, *96*, 16103.

(6) Shaevitz, J. W.; Fletcher, D. A. Load Fluctuations Drive Actin Network Growth. *Proc. Natl. Acad. Sci.* **2007**, *104*, 15688−15692.

(7) Nguyen, T. D.; Hogue, I. B.; Cung, K.; Purohit, P. K.; McAlpine, M. C. Tension-Induced Neurite Growth in Microfluidic Channels. *Lab Chip* **2013**, *13*, 3735.

(8) Gosvami, N. N.; Bares, J. A.; Mangolini, F.; Konicek, A. R.; Yablon, D. G.; Carpick, R. W. Mechanisms of Antiwear Tribofilm Growth Revealed in Situ by Single-Asperity Sliding Contacts. *Science* **2015**, *348*, 102−106.

(9) Tang, Y.; Zhang, Y.; Deng, J.; Wei, J.; Tam, H. L.; Chandran, B. K.; Dong, Z.; Chen, Z.; Chen, X. Mechanical Force-Driven Growth of Elongated Bending TiO2-based Nanotubular Materials for Ultrafast Rechargeable Lithium Ion Batteries. *Adv. Mater.* **2014**, *26*, 6111−6118.

(10) Balakrishnan, V.; Bedewy, M.; Meshot, E. R.; Pattinson, S. W.; Polsen, E. S.; Laye, F.; Zakharov, D. N.; Stach, E. A.; Hart, A. J. Real-Time Imaging of Self-Organization and Mechanical Competition in Carbon Nanotube Forest Growth. *ACS Nano* **2016**, *10*, 11496−11504.

(11) Bedewy, M.; Meshot, E. R.; Reinker, M. J.; Hart, A. J. Population Growth Dynamics of Carbon Nanotubes. *ACS Nano* **2011**, *5*, 8974−8989.

(12) Maschmann, M. R. Integrated Simulation of Active Carbon Nanotube Forest Growth and Mechanical Compression. *Carbon* **2015**, *86*, 26−37.

(13) Bedewy, M.; Hart, A. J. Mechanical Coupling Limits the Density and Quality of Self-Organized Carbon Nanotube Growth. *Nanoscale* **2013**, *5*, 2928.

(14) Bedewy, M.; Meshot, E. R.; Guo, H.; Verploegen, E. A.; Lu, W.; Hart, A. J. Collective Mechanism for the Evolution and Self-Termination of Vertically Aligned Carbon Nanotube Growth. *J. Phys. Chem. C* **2009**, *113*, 20576−20582.

(15) Ginga, N. J.; Chen, W.; Sitaraman, S. K. Waviness Reduces Effective Modulus of Carbon Nanotube Forests by Several Orders of Magnitude. *Carbon* **2014**, *66*, 57−66.

(16) Jakubinek, M. B.; White, M. A.; Li, G.; Jayasinghe, C.; Cho, W.; Schulz, M. J.; Shanov, V. Thermal and Electrical Conductivity of Tall, Vertically Aligned Carbon Nanotube Arrays. *Carbon* **2010**, *48*, 3947−3952.

(17) Ivanov, I.; Puretzky, A.; Eres, G.; Wang, H.; Pan, Z.; Cui, H.; Jin, R.; Howe, J.; Geohegan, D. B. Fast and Highly Anisotropic Thermal Transport through Vertically Aligned Carbon Nanotube Arrays. *Appl. Phys. Lett.* **2006**, *89*, 223110.

(18) Hart, A. J.; Slocum, A. H. Force Output, Control of Film Structure, and Microscale Shape Transfer by Carbon Nanotube Growth under Mechanical Pressure. *Nano Lett.* **2006**, *6*, 1254−1260.

(19) Han, J.-H.; Graff, R. A.; Welch, B.; Marsh, C. P.; Franks, R.; Strano, M. S. A Mechanochemical Model of Growth Termination in Vertical Carbon Nanotube Forests. *ACS Nano* **2008**, *2*, 53−60.

(20) Plata, D. L.; Meshot, E. R.; Reddy, C. M.; Hart, A. J.; Gschwend, P. M. Multiple Alkynes React with Ethylene to Enhance Carbon Nanotube Synthesis, Suggesting a Polymerization-like Formation Mechanism. *ACS Nano* **2010**, *4*, 7185−7192.

DOI: 10.1021/acs.chemmater.8b03627
Chem. Mater. 2019, 31, 407−418

(21) Glatter, O.; Kratky, O. *Small Angle X-Ray Scattering*; Academic Press Inc: New York, NY, 1982.
(22) Cao, A.; Dickrell, P. L.; Sawyer, W. G.; Ghasemi-Nejhad, M. N.; Ajayan, P. M. Super-Compressible Foamlike Carbon Nanotube Films. *Science* **2005**, *310*, 1307−1310.
(23) Hutchens, S. B.; Needleman, A.; Greer, J. R. Analysis of Uniaxial Compression of Vertically Aligned Carbon Nanotubes. *J. Mech. Phys. Solids* **2011**, *59*, 2227−2237.
(24) Gibson, L. J.; Ashby, M. F. *Cellular Solids, Structure and Properties*; Pergamon Press: Elmsford, NY, 1988.
(25) Peng, B.; Locascio, M.; Zapol, P.; Li, S.; Mielke, S. L.; Schatz, G. C.; Espinosa, H. D. Measurements of Near-Ultimate Strength for Multiwalled Carbon Nanotubes and Irradiation-Induced Crosslinking Improvements. *Nat. Nanotechnol.* **2008**, *3*, 626−631.
(26) Liang, X.; Shin, J.; Magagnosc, D.; Jiang, Y.; Jin Park, S.; John Hart, A.; Turner, K.; Gianola, D. S.; Purohit, P. K. Compression and Recovery of Carbon Nanotube Forests Described as a Phase Transition. *Int. J. Solids Struct.* **2017**, *122*−*123*, 196−209.
(27) van Wyk, C. M. 20-Note on the Compressibility of Wool. *J. Text. Inst., Trans.* **1946**, *37*, T285−T292.
(28) Toll, S. Packing Mechanics of Fiber Reinforcements. *Polym. Eng. Sci.* **1998**, *38*, 1337−1350.
(29) Puretzky, A. A.; Geohegan, D. B.; Jesse, S.; Ivanov, I. N.; Eres, G. In Situ Measurements and Modeling of Carbon Nanotube Array Growth Kinetics during Chemical Vapor Deposition. *Appl. Phys. A* **2005**, *81*, 223−240.
(30) Meshot, E. R.; Plata, D. L.; Tawfick, S.; Zhang, Y.; Verploegen, E. A.; Hart, A. J. Engineering Vertically Aligned Carbon Nanotube Growth by Decoupled Thermal Treatment of Precursor and Catalyst. *ACS Nano* **2009**, *3*, 2477−2486.
(31) Lee, Y. T.; Park, J.; Choi, Y. S.; Ryu, H.; Lee, H. J. Temperature-Dependent Growth of Vertically Aligned Carbon Nanotubes in the Range 800−1100 °C. *J. Phys. Chem. B* **2002**, *106*, 7614−7618.
(32) Liu, K.; Jiang, K.; Feng, C.; Chen, Z.; Fan, S. A Growth Mark Method for Studying Growth Mechanism of Carbon Nanotube Arrays. *Carbon* **2005**, *43*, 2850−2856.
(33) Bronikowski, M. J. Longer Nanotubes at Lower Temperatures: The Influence of Effective Activation Energies on Carbon Nanotube Growth by Thermal Chemical Vapor Deposition. *J. Phys. Chem. C* **2007**, *111*, 17705−17712.
(34) Dresselhaus, M. S.; Dresselhaus, G.; Saito, R. Physics of Carbon Nanotubes. *Carbon* **1995**, *33*, 883−891.
(35) Rao, A.; Tawfick, S.; Bedewy, M.; Hart, A. J. Morphology-Dependent Load Transfer Governs the Strength and Failure Mechanism of Carbon Nanotube Yarns. *Extreme Mech. Lett.* **2016**, *9*, 55−65.
(36) Meshot, E. R.; Bedewy, M.; Lyons, K. M.; Woll, A. R.; Juggernauth, K. A.; Tawfick, S.; Hart, A. J. Measuring the Lengthening Kinetics of Aligned Nanostructures by Spatiotemporal Correlation of Height and Orientation. *Nanoscale* **2010**, *2*, 896.
(37) Abécassis, B.; Testard, F.; Spalla, O.; Barboux, P. Probing in Situ the Nucleation and Growth of Gold Nanoparticles by Small-Angle X-Ray Scattering. *Nano Lett.* **2007**, *7*, 1723−1727.
(38) Liu, J.; Pancera, S.; Boyko, V.; Shukla, A.; Narayanan, T.; Huber, K. Evaluation of the Particle Growth of Amorphous Calcium Carbonate in Water by Means of the Porod Invariant from SAXS. *Langmuir* **2010**, *26*, 17405−17412.

DOI: 10.1021/acs.chemmater.8b03627
Chem. Mater. 2019, 31, 407−418